

A study on the microscopic mechanism of methanesulfonic acid-promoted binary nucleation of sulfuric acid and water

Hui Wen^a, Teng Huang^a, Chun-Yu Wang^a, Xiu-Qiu Peng^a, Shuai Jiang^b, Yi-Rong Liu^b, Wei Huang^{a,b,c,*}

^a Laboratory of Atmospheric Physico-Chemistry, Anhui Institute of Optics & Fine Mechanics, Chinese Academy of Sciences, Hefei, Anhui, 230031, China

^b School of Information Science and Technology, University of Science and Technology of China, Hefei, Anhui, 230026, China

^c Center for Excellence in Urban Atmospheric Environment, Institute of Urban Environment, Chinese Academy of Sciences, Xiamen, Fujian, 361021, China

ARTICLE INFO

Keywords:

Microscopic mechanism
Methanesulfonic acid
Sulfuric acid–water
Ternary nucleation
Atmospheric relevance
Evaporation rate

ABSTRACT

Methanesulfonic acid (MSA) is believed to play an important role in the formation and growth of atmospheric organic aerosols and could facilitate the binary nucleation of sulfuric acid (SA)–water (W). However, understanding of larger clusters formed by gas-phase MSA with atmospheric nucleation precursors from microscopic aspect is lacking. In this work, to study the microscopic mechanism of the ternary nucleation, the structural characteristics and thermodynamics of MSA clusters with SA in the presence of up to six W molecules have been investigated. It was found that MSA forms relatively stable clusters with SA and W molecules and that acid dissociation plays an important role. The analysis of the atmospheric relevance indicates that the heterodimer MSA–SA and monohydrated cluster MSA–SA–W₁ show an obvious relative concentration in the atmosphere, and thus, these species likely participate in new particle formation (NPF). However, with an increasing number of W molecules, the concentration of clusters gradually decreases. Additionally, the minimum energy isomer of MSA–SA–W₄ is predicted to possess a relatively stable configuration under the employed temperature dependence analysis, and evaporation rate analysis. The detailed non-covalent interactions of MSA–SA–W_n, n = 3–6 cluster have been thoroughly studied for the first time.

1. Introduction

Aerosols have a significant effect on humankind via their influence on weather, climate, and health quality (Molina et al., 1997; Zhang et al., 2007). They can be directly emitted into the atmosphere from natural and anthropogenic sources or formed via the nucleation from gas-phase species in the atmosphere (Charlson et al., 1992; Kulmala, 2003). New particle formation (NPF) produces a large fraction of atmospheric aerosols, and typical NPF events occur in two distinct stages (Wang et al., 2010; Zhang, 2010; Zhang et al., 2012): (1) nucleation to form the critical nucleus (with maximum free energy), and (2) subsequent growth of the critical nucleus to a detectable size (2–3 nm) that competes with the capture and removal of the critical cluster by coagulation with pre-existing aerosols.

Sulfuric acid (H₂SO₄, SA) has been widely identified as a major atmospheric nucleating species (Zhang, 2010; Zheng et al., 2010). The homogeneous nucleation of SA and water (H₂O, W) has been long considered as the primary pathway for the source of NPF in the atmosphere. However, growing evidence (O'Dowd et al., 1999; Aalto et al.,

2001) indicates that this binary nucleation is not sufficient to explain the measured nucleation rates in an actual atmospheric environment. Therefore, third substances, which are involved in nucleation phenomena, have been proposed (Kulmala and Kerminen, 2008; Kuang et al., 2010; Paasonen et al., 2010). However, along with enhancement processes for nucleation science, the nucleation routes for these third substances are still open to critical discussion.

Atmospheric observations have revealed that aerosols often contain a number of organic carbonyls and acids, some of which may participate in nucleation and growth to form nanoparticles thereafter (Zhang et al., 2004, 2009; Zhao et al., 2005, 2006; 2009; Fan et al., 2006; Nadykto and Yu, 2007; Wang et al., 2010). Recent studies have also shown that the presence of organic acids could be considered as a source of aerosol nucleation intermediates and catalytic agents to enhance the nucleation of the SA–W system via the formation of strongly hydration-bonded clusters (Zhang et al., 2004, 2009; Nadykto and Yu, 2007; McGraw and Zhang, 2008; Zhao et al., 2009; Zhang, 2010). So far, theoretical study of the effects of different kinds of organic acids on NPF have been thoroughly investigated, including studies on the effects

* Corresponding author. School of Information Science and Technology, University of Science and Technology of China, Hefei, Anhui, 230026, China.
E-mail address: Huangwei6@ustc.edu.cn (W. Huang).

of benzoic acid, toluic acid, different monocarboxylic acids, and dicarboxylic acids (Weber et al., 2012; Xu and Zhang, 2012; Zhu et al., 2014; Miao et al., 2015).

However, there is another potentially important species generated alongside SA in the oxidation of organosulfur compounds, such as dimethyl sulfide and methyl mercaptan, in air: methanesulfonic acid ($\text{CH}_3\text{SO}_3\text{H}$, MSA). Gas-phase MSA has been measured in air at concentrations that are typically approximately 10–100% of coexisting gas-phase SA (Eisele and Tanner, 1993). There is evidence that MSA primarily contributes to particle growth in the atmosphere (Kreidenweis and Seinfeld, 1988; Kreidenweis et al., 1989; Wyslouzil et al., 1991a,b; Vandingenen and Raes, 1993) and contributes to NPF (Dawson et al., 2012). Okuyama and coworkers (Wyslouzil et al., 1991a) have systematically studied the temperature dependence of MSA–W binary nucleation using a continuous flow mixing-type device and found that under-saturated MSA vapor in the presence of moderate relative humidity (RH) (less than 60%) can generate observed aerosol concentrations up to approximately 10^5 cm^{-3} .

A recent study by Bork et al. revealed that MSA could enhance formation rates of molecular clusters of SA and dimethyl amine (DMA) by up to one order of magnitude (Bork et al., 2014). Tao and coworkers investigated the MSA– NH_3 – $\text{W}_{0.4}$ system by quantum chemical calculations and found that ionization dissociation plays an important role (Li et al., 2007b). In particular, the Finlayson-Pitts group conducted extensive work (Ezell et al., 2010; Dawson et al., 2012; Chen et al., 2015) to study NPF events from the reactions of MSA with ammonia/amines as a function of RH and precursor concentrations using a slow aerosol flow system. They demonstrated that MSA and amines form particles, and W plays a major role. In addition, different amines showed different dependencies on W vapor and precursor concentrations in a complex manner; methylamine was the most effective at forming new particles, and ammonia was the least efficient of all precursors.

Most studies have focused on the reaction of MSA with ammonia/ amines, while little is known about the interaction of MSA with SA and W molecules. So far, only one report conducted by Dingenen and coworkers (Vandingenen and Raes, 1993) has concentrated on MSA–SA–W ternary nucleation, and they found that, at a fixed temperature (298.15 K), the addition of MSA to an SA–W mixture in the gas phase increases the nucleation rate using simplified classical nucleation theory. However, the microscopic mechanism of nucleation, such as the detail structural characteristics or the physical chemistry properties of the hydration of MSA with SA, is poorly understood, especially for larger clusters with a high number of W molecules.

Herein, the hydration of MSA–SA is studied using density functional theory (DFT) at the PW91PW91/6–311++G (3df, 3pd) level. The minima energy structures of MSA–SA– W_n ($n = 0$ –6) were found, and the thermodynamic properties of these clusters were determined. The temperature dependences and the nature of acid dissociation at the molecular level were further studied. In addition, the evaporation rate of the hydrates and its atmospheric relevance were also investigated to gain further insight into the ternary nucleation. This work is a continuation of longstanding efforts to investigate the microscopic mechanisms of atmospheric nucleation, molecule–molecule interactions, hydrogen-bonded interactions, water cluster formation, and atmospheric processes.

2. Methodology

The initial geometries of the monomers and MSA–SA– W_n ($n = 0$ –6) clusters were obtained with the Basin–Hopping (BH) algorithm coupled with density functional theory (DFT). The generalized gradient–corrected Perdew–Burke–Ernzerhof (PBE) (Perdew et al., 1996) exchange correlation functional and the double numerical plus d-functions (DND) basis set with effective core potentials (ECPs), implemented in DMol³ (Delley, 1990), were used with a medium level convergence criterion to optimize the structures. This method was

highly efficient to explore atomic and molecular systems in our previous studies (Wen et al., 2013, 2014; 2016; Liu et al., 2014).

Hundreds of structures were sampled according to the cluster sizes. The isomers for each cluster were ranked according to their relative energies. The top twenty isomers in each case were selected and further optimized at the Perdew and Wang's 1991 functional (PW91) (Perdew et al., 1996) together with the 6–311++G (3df, 3pd) basis set (Raghavachari and Trucks, 1989). For the larger size clusters, a two-step optimization method was employed. The low-lying isomers were first optimized at the PW91PW91/6–311++G (d, p) level, and then, the stable clusters from the first optimization were further optimized at the PW91PW91/6–311++G (3df, 3pd) level of theory to get the final configurations. PW91 method has the fine performance on a large number of atmospheric cluster containing SA, W, and the common organic acids, including predictions of structural characteristics, the thermodynamics of cluster formation, and satisfactory similarity compared with experimental results (Nadykto and Yu, 2007). Harmonic vibrational frequencies were calculated to confirm that the obtained isomers were the true minima. The convergence criteria were the default settings in the Gaussian 09 suite of programs (Frisch et al., 2009).

Single point energy calculations were performed at a higher level of theory, i.e., second-order Møller–Plesset perturbation theory with explicitly correlated methods with density fitting (DF–MP2–F12) with the Pople's all electron basis set 6–311++G (3df, 3pd). The DF–MP2–F12 calculations were performed using Molpro 2010.1 (Werner et al., 2010). The thermodynamic corrections obtained at PW91PW91/6–311++G (3df, 3pd) were combined with the DF–MP2–F12 single point energies to evaluate the zero-point corrected energies (ZPE) and other thermodynamic parameters.

3. Results and discussion

3.1. Conformational analysis

The most stable isomers of each monomer and heterodimer were obtained at the PW91 level with the 6–311++G (3df, 3pd) basis set using the Gaussian 09 package. The calculated geometry of SA possesses C_2 symmetry and that of W possesses C_{2v} symmetry, consistent with those described by Zhang et al. (Zhao et al., 2009; Xu and Zhang, 2012). Intramolecular O–H–O hydrogen bonds (HB) are found in the stable conformations of the MSA and SA monomer, as shown in Fig. 1. The strength of the intramolecular HB of MSA (2.39 Å) is larger than the HB of SA (2.48 Å). The free O–H bond lengths in the MSA, SA, and W monomer are almost identical. On the basis of the monomers, the heterodimer molecular complexes are constructed and optimized. The stable conformations of the heterodimer MSA–W and SA–W are consistent with previous studies (Dawson et al., 2012; Xu and Zhang, 2013). A pair of intermolecular HBs is formed between the MSA/SA and W. The MSA/SA molecule acts both as an HB donor and as an HB acceptor: the donor moiety forms a relatively weak HB, and the acceptor part forms a stronger HB at the expense of the O–H bond strength. Three strong intermolecular HBs are found between the MSA–SA heterodimer without the formation of a free OH group. Instead, the strengthening of the intermolecular HBs can be inferred from the lengthening of the adjacent O–H bonds. That is, the adjacent O–H bond lengths in the heterodimer are larger than those in the monomers.

The optimized structures of the global and several selected local minima at the PW91PW91/6–311++G (3df, 3pd) level of theory for MSA–SA– W_n ($n = 1$ –6) that will be discussed in this section are shown in Fig. 2. More local minima could be seen in Figs. S1–10 in the Supplementary Data. The representations of these structures are defined using “ n - i (x) p ” notation. In this notation, “ n ” ($n = \text{I–VI}$) represents the number of W molecules, and “ i ” ($i = \text{a–bz}$), displayed in order of increasing electronic energy at 0 K for each cluster size, denotes the different isomers with the same value of n . The index “ x ” ($x = \text{N, MSA, SA, and MSA\&SA}$) is utilized to distinguish the different acid-dissociated

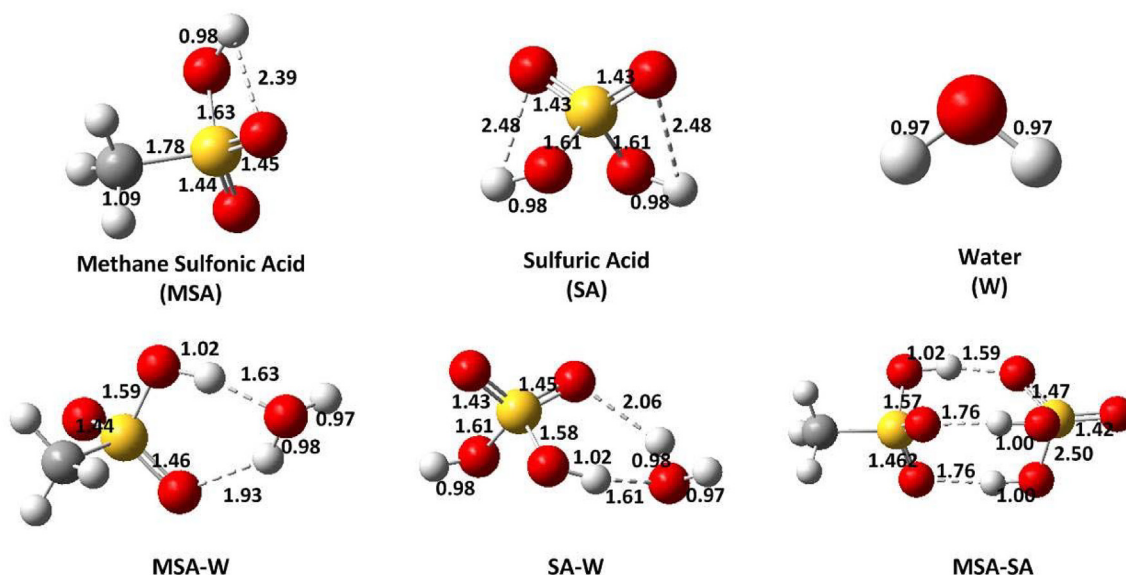


Fig. 1. Optimized geometries of the monomers and the heterodimers at the PW91PW91/6–311 + + G (3df, 3pd) level of theory. (Red for oxygen, white for hydrogen, gray for carbon, and yellow for sulfur). (For interpretation of the references to color in this figure legend, the reader is referred to the Web version of this article.)

models of the clusters. The structures are labeled “N” if the clusters remain neutral as MSA-SA-W_n , “MSA” if only MSA undergoes acid dissociation to form di-ionic $\text{MSA}^- \text{-SA-W}^+ \text{-W}_{n-1}$ clusters, “SA” if only SA undergoes acid dissociation to form di-ionic $\text{MSA-SA}^- \text{-W}^+ \text{-W}_{n-1}$ clusters, and “MSA&SA” if both acids undergo their first acid dissociation to form tetra-ionic $\text{MSA}^- \text{-SA}^- \text{-(W}_2\text{)}^+ \text{-W}_{n-2}$ clusters. The “p” ($p = 3\text{--}13$) indicates the number of intermolecular HBs formed in the cluster.

For the smallest ternary clusters, MSA-SA-W_1 , the minimum-energy isomer (I-a) possesses a cyclic-shape configuration, where the W monomer is located above the MSA-SA heterodimer, and one of the strong HB of the MSA-SA heterodimer is broken. W binds to SA with a strong HB (1.51 Å) and to MSA with a relatively weak HB (1.79 Å); however, both HBs are stronger than those in the heterodimer SA-W (1.61 Å) and MSA-W (1.93 Å). The competing isomer I-b possesses a linear shape, which is approximately 3 kcal mol⁻¹ higher in energy than isomer I-a at both the PW91 and DF-MP2-F12 methods. Acid dissociation is not observed for either acid.

For the MSA-SA-W_2 complexes, di-ionic structures II-a (SA) and II-c (MSA) are found as low-lying isomers, illustrating that deprotonation of the acid molecules can begin even when only two W molecules are added. The isomer II-a, which is based on the I-a and MSA-SA dimer, the newly added W breaks the second HB between the MSA-SA dimer, resulting in the deprotonation of SA forming SA^- and W^+ ions. The competing isomer II-b with five HBs remains neutral, and no acid dissociation is found. In isomer II-c, deprotonation of MSA occurs; however, this isomer is less stable (1.66 kcal mol⁻¹) than the di-ionic cluster of deprotonated SA.

Starting from the MSA-SA-W_3 clusters, the minimum energy isomers of the relatively larger sized clusters are all tetra-ionic configurations, indicating that both acids readily undergo dissociation when more W molecules are added. Similarly, the minimum energy isomer of MSA-SA-W_3 (III-a), which is based on the structure of I-a, II-a, and MSA-SA dimer, the newly added W breaks the third HB between the MSA-SA dimer. The isomer has a clear tetra-ionic geometry with simultaneously deprotonated MSA and SA forming MSA^- , SA^- , and W^+ ions where the hydronium and W molecules bridge MSA^- and SA with a network of seven HBs. This isomer suggests that a new structural motif emerges when more W molecules are added.

For the MSA-SA-W_4 clusters, the tetra-ionic configuration of isomer IV-a is an evolution from isomer III-a, where the fourth W is bound to

one of the oxygen atoms in both MSA and SA, forming a pan-shaped structure. In this system, the di-ionic isomer of deprotonated MSA (IV-d) is slightly stable than that of deprotonated SA (IV-e), whereas the neutral isomer (IV-av) is much higher in energy than the minimum isomer.

In the clusters of MSA-SA-W_5 , the lowest electronic energy structure at both PW91 and DF-MP2-F12 methods is V-a, which is a tetra-ionic configuration with eleven HBs. As shown in Figs. S7 and S8 in the Supplementary Data, the tetra-ionic configurations are more stable than those of the di-ionic structures of deprotonated MSA/SA and the neutral clusters. The pan-shaped configuration is also found for isomers V-e and V-k.

For the system of MSA-SA-W_6 , the most stable structure (VI-a) forms a strong and stable quasi-hollow-cuboid configuration with three tandem W molecules as the long side. The structure can also be viewed as the combination of ionic MSA^- and SA^- separated by two hydroniums and four W molecules. There are no neutral clusters found in this system, suggesting that ionization of the clusters is preferred when more W molecules are added. The pan-shaped structures are also found in isomers VI-f and VI-l, which are less stable than the minimum isomer.

In general, structures with more HBs are more stable for each species. Starting from the MSA-SA-W_2 complexes, acid dissociation begins to occur. Both acids undergo dissociation to form tetra-ionic structures when more W molecules are added. The tetra-ionic clusters are more stable than the di-ionic clusters, and the neutral cluster has the lowest population. Considering geometry, two types of geometries are generally presented: surface type and interior type. The neutral clusters are more favorable in the surface-type configurations. Unlike simple molecular clusters, such as $\text{IO}_3^-(\text{H}_2\text{O})_n$ (Wen et al., 2013) or $\text{HCO}_3^-(\text{H}_2\text{O})_n$ (Wen et al., 2016) clusters, the current species favor the interior-type geometries. In addition, the hydronium in the di-ionic isomer favors the formation of bridging structures, where the hydronium ion locates inside and donates three HBs.

3.2. Thermodynamics: stepwise hydration

The thermodynamic corrections obtained at PW91PW91/6–311 + + G (3df, 3pd) are combined with the DF-MP2-F12 single-point energies to evaluate the zero-point corrected energies (ZPE) and other thermodynamic parameters. The calculated binding energies with zero-point energy (ZPE) correction (ΔE_e^{OK}) at 0 K, binding energies without

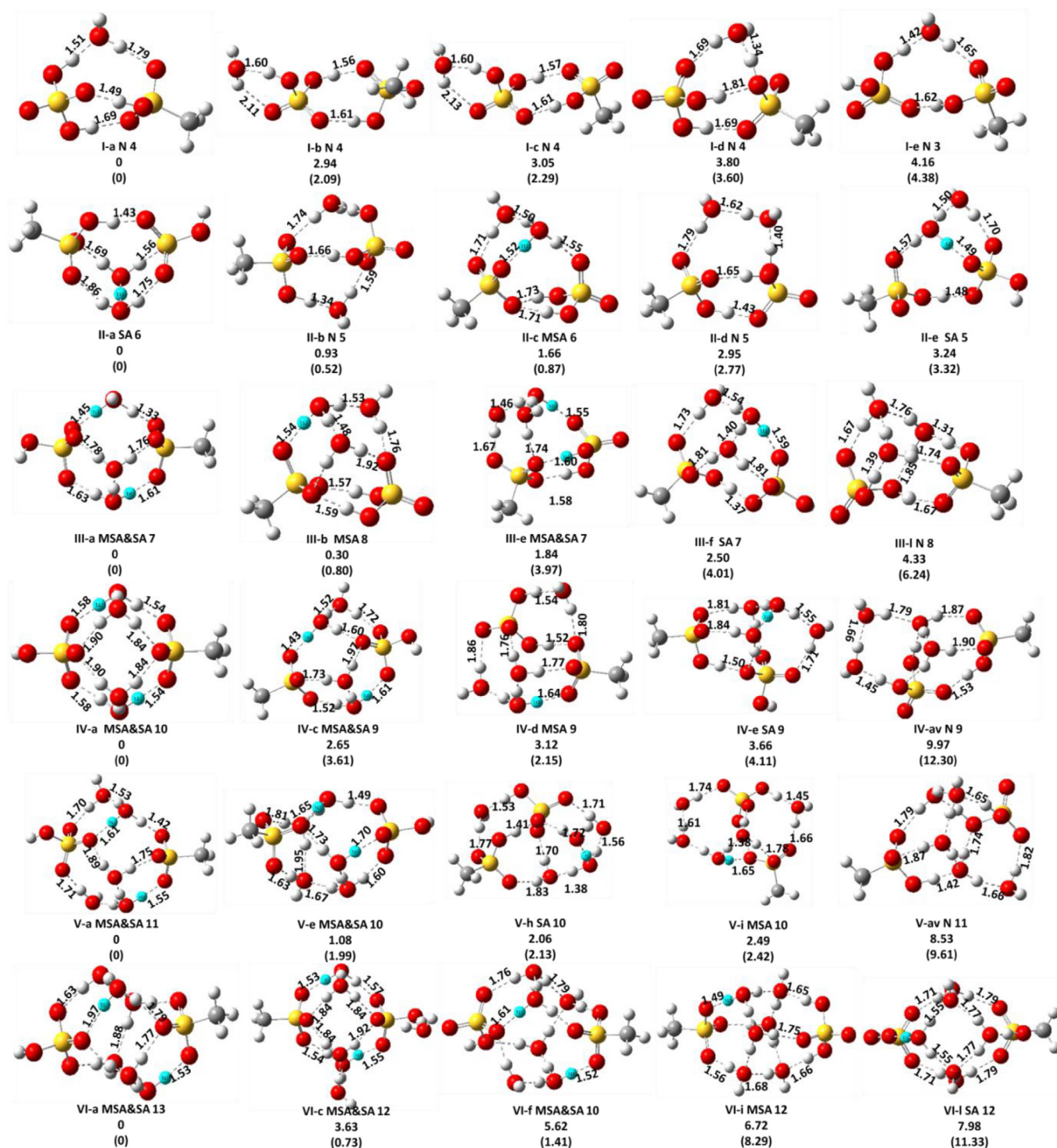


Fig. 2. Optimized geometries of the MSA-SA-W_n clusters (n = 1–6) at the PW91PW91/6-311++G(3df, 3pd) level of theory, ordered by increasing relative electronic energy (in kcal mol⁻¹). The relative energies in parenthesis are calculated under the DF-MP2-F12/6-311++G(3df, 3pd) method. (Red for oxygen, white for hydrogen, gray for carbon, yellow for sulfur, and blue for transferred proton). (For interpretation of the references to color in this figure legend, the reader is referred to the Web version of this article.)

ZPE corrections (ΔE_0^{0K}) at 0 K, and the thermodynamic parameters, including thermal energies ($\Delta U^{298.15K}$), enthalpies ($\Delta H^{298.15K}$), and Gibbs free energies ($\Delta G^{298.15K}$) at 298.15 K, for isomers of the MSA-SA-W₀₋₆ clusters are given in Table 1 and Tables S1–S5 in the Supplementary Data. The binding energies are calculated using the following equation:

$$\Delta E_n = E_n - E_{MSA} - E_{SA} - n \times E_W \quad (1)$$

All thermodynamic parameters were calculated in a similar way. As shown in Table 1 and Tables S1–S5 in the Supplementary Data, the thermodynamic parameters decrease monotonously with an increasing number of W clusters. The relative binding energies (ΔE) are negative, implying that the stepwise hydration of MSA-SA is an exothermic reaction and indicating that the reaction occurs from an unstable substance to a stable substance. The Gibbs free energy change ($\Delta G = G_n - G_{MSA} - G_{SA} - n \times G_W$) value is the most important

Table 1

Binding energies at 0 K (ΔE_e^{0K}), ZPE-corrected binding energies at 0 K (ΔE_0^{0K}), thermal energies at 298.15 K ($\Delta U^{298.15K}$), enthalpies at 298.15 K ($\Delta H^{298.15K}$), and Gibbs free energies at 298.15 K ($\Delta G^{298.15K}$) for the selected isomers of the MSA-SA- W_n , $n = 0-6$ clusters (in kcal mol⁻¹).

Isomers	ΔE_e^{0K}	ΔE_0^{0K}	$\Delta U^{298.15K}$	$\Delta H^{298.15K}$	$\Delta G^{298.15K}$
Dimer (N)	-21.28	-19.69	-19.83	-20.43	-6.72
I-a (N)	-35.64	-32.21	-32.57	-33.75	-10.09
II-a (SA)	-49.87	-44.57	-45.46	-47.24	-12.96
II-b (N)	-48.94	-43.98	-44.54	-46.32	-13.18
II-c (MSA)	-48.22	-41.81	-42.76	-44.53	-9.95
III-a (MSA&SA)	-65.85	-57.05	-58.36	-60.73	-15.34
III-b (MSA)	-65.55	-56.81	-58.06	-60.43	-15.27
III-f (SA)	-63.35	-55.82	-56.83	-59.20	-14.54
III-l (N)	-61.52	-53.95	-55.27	-57.64	-11.77
IV-a (MSA&SA)	-81.86	-70.51	-72.31	-75.27	-18.89
IV-d (MSA)	-78.75	-67.89	-69.45	-72.41	-16.02
IV-e (SA)	-78.21	-67.14	-68.42	-71.38	-16.03
IV-av (N)	-71.90	-62.46	-63.50	-66.46	-12.55
V-a (MSA&SA)	-93.26	-79.81	-82.20	-85.75	-19.41
V-i (MSA)	-90.76	-78.21	-79.78	-83.33	-18.43
V-k (SA)	-89.63	-77.38	-78.85	-82.40	-17.20
V-av (N)	-84.72	-71.71	-73.47	-77.02	-10.68
VI-a (MSA&SA)	-108.41	-93.11	-95.79	-98.94	-22.28
VI-l (MSA)	-103.69	-87.27	-89.84	-93.98	-16.49
VI-l (SA)	-102.43	-87.62	-90.15	-94.30	-17.56

¹Thermodynamic parameters are calculated at the PW91PW91/6-311 + G (3df, 3pd) level of MSA-SA- W_n ($n = 0-6$) via the reaction MSA + SA → MSA-SA or MSA + SA + $n \times W \rightarrow$ MSA-SA- W_n ($n = 1-6$).

parameter of the system to the environment; a negative value of ΔG in each cluster size indicates that the reaction will occur spontaneously, and a smaller ΔG value represents a more stable isomer.

A trend in stepwise enthalpies (ΔH) can be inferred by considering the number of newly formed HBs at each hydration step. In the current study, from the MSA-SA- W_0 cluster to the MSA-SA- W_6 cluster, the numbers of newly formed HBs for the minimum energy isomer of each species are 1, 1, 2, 3, 1, and 2, respectively, for the sequence of steps. Three new HBs are formed at MSA-SA- W_4 cluster size, resulting in a relatively stable configuration when compared to the other complexes. This extra stabilization could be due to the construction of the compact pan-shaped configuration with four W monomers sitting between the MSA-SA dimer. That is, the formation of HBs in the MSA-SA- W_n complexes leads to cluster stabilization, as HBs are not only formed between solute and solvent molecules but also among W molecules themselves. Compared with the prior cluster size, the additional W monomer could weaken the solute-solvent interactions, and, thus the stepwise ΔH values may gradually decrease with the increase of the cluster size.

Meanwhile, the magnitudes of all the studied thermodynamic parameter changes for the minimum structure of each cluster sizes at each hydration steps are shown in Table 2. It can be clearly seen that the magnitudes of all the thermodynamic parameter changes at MSA-SA- W_4 are greater among all the hydration steps, which may indicate that the MSA-SA- W_4 cluster has special characteristics or stabilities.

Table 2

The magnitude of the thermodynamic parameter changes Binding energy changes at 0 K ($\Delta \Delta E_e^{0K}$), ZPE-corrected binding energy changes at 0 K ($\Delta \Delta E_0^{0K}$), thermal energy changes at 298.15 K ($\Delta \Delta U^{298.15K}$), enthalpy changes at 298.15 K ($\Delta \Delta H^{298.15K}$), and Gibbs free energy changes at 298.15 K ($\Delta \Delta G^{298.15K}$) for the minimum structures of the MSA-SA- W_n , $n = 0-6$ clusters at each hydration steps (in kcal mol⁻¹).

	$\Delta \Delta E_e^{0K}$	$\Delta \Delta E_0^{0K}$	$\Delta \Delta U^{298.15K}$	$\Delta \Delta H^{298.15K}$	$\Delta \Delta G^{298.15K}$
(MSA-SA- W_1)-(MSA-SA)	-14.36	-12.52	-12.74	-13.32	-3.37
(MSA-SA- W_2)-(MSA-SA- W_1)	-14.23	-12.36	-12.89	-13.49	-2.87
(MSA-SA- W_3)-(MSA-SA- W_2)	-15.98	-12.48	-12.9	-13.49	-2.38
(MSA-SA- W_4)-(MSA-SA- W_3)	-16.01	-13.46	-13.95	-14.54	-3.55
(MSA-SA- W_5)-(MSA-SA- W_4)	-11.40	-9.30	-9.89	-10.48	-0.52
(MSA-SA- W_6)-(MSA-SA- W_5)	-15.15	-13.3	-13.59	-13.19	-2.87

3.3. Acid dissociation

The nature of acids in an aqueous environment is fundamental to many aspects of chemistry. The defining feature of an acid is its ability to transfer a proton to water, i.e., acid dissociation, which is a significant topic and has attracted much attention (Robertson and Johnson, 2002; Gutberlet et al., 2009; Forbert et al., 2011; Leopold, 2011; Temelso et al., 2012a,b). In the current study, we focused on the dissociation of hydrated MSA compounded with SA.

The relative binding energies and stepwise Gibbs free energy changes were calculated for each cluster size via the MSA-SA- $W_{n-1} + W \rightarrow$ MSA-SA- W_n pathway and are marked as ΔE^2 and ΔG^2 , respectively, as shown in Fig. 3. ΔC_n^i In Fig. 3(a), the MSA-SA heterodimer and a single W cluster remain undissociated. The first deprotonation of MSA or SA emerges once the second W is added to the MSA-SA- W_1 complex, and the di-ionic cluster of deprotonated SA is slightly more stable than the completely neutral moieties or the di-ionic cluster of deprotonated MSA. Starting from the MSA-SA- W_3 complex, upon the addition of more W molecules ($n = 3-6$), the MSA and SA dissociate simultaneously. Moreover, the tetra-ionic clusters are more stable than the di-ionic clusters and neutral moieties in each species except for the MSA-SA- W_3 complex. This indicates that the acid dissociation event exists in the formation of the MSA-SA- W_n cluster and plays an important role in the stability of this system, i.e., acid dissociation, as one kind of proton transfer, leads to a stable cluster.

In Fig. 3 (b), the general trend of ΔG^2 is similar to that of $\Delta E^2 \Delta C_n^i$ (Fig. 3 (a)); the neutral moieties have unfavorable thermodynamics as the number of W molecules increase, while the tetra-ionic clusters are favorable at the size of $n = 3-6$ at 298.15 K. The di-ionic clusters of deprotonated SA are slightly more favorable than those of deprotonated MSA, except for the MSA-SA- W_3 complex. This does not indicate that the ionic clusters with MSA are difficult to form but instead indicates that the ionic clusters with MSA exist in equilibrium with the di-ionic clusters of deprotonated SA at nearly equal numbers. The exact values may depend on the initial concentrations of MSA, SA, and W as well as the temperature. Furthermore, the results also predict that these three acid dissociated models (MSA, SA and MSA&SA) could coexist in the atmosphere, especially when more W molecules are present.

Previously, a study (Temelso et al., 2012b) of the SA- W_n ($n = 1-6$) system showed that the ionic SA⁻W⁺- W_{n-1} clusters are less stable than the neutral SA- W_n clusters for $n < 3$ and become the global minima when $n > 4$. Ionic dissociation of MSA in clusters with small numbers of W molecules (MSA- W_{1-5}) was studied by Tao et al. (Li et al., 2007a), and they found that a minimum of four W molecules was required for MSA to dissociate and form the MSA anion. According to our study of the MSA-SA- W_n ($n = 0-6$) clusters, the ionic clusters are more stable than the neutral clusters for $n > 2$ in terms of both ΔE^2 (0 K) and ΔG^2 (298.15 K). This indicates that the ternary system is greatly promotes the acid dissociation compared with the binary system, which is similar to oxalic acid (OA) with the SA-W clusters (Miao et al., 2015). These findings can help understand the organics-enhanced nucleation between atmospheric nucleation precursors and MSA. In addition, the

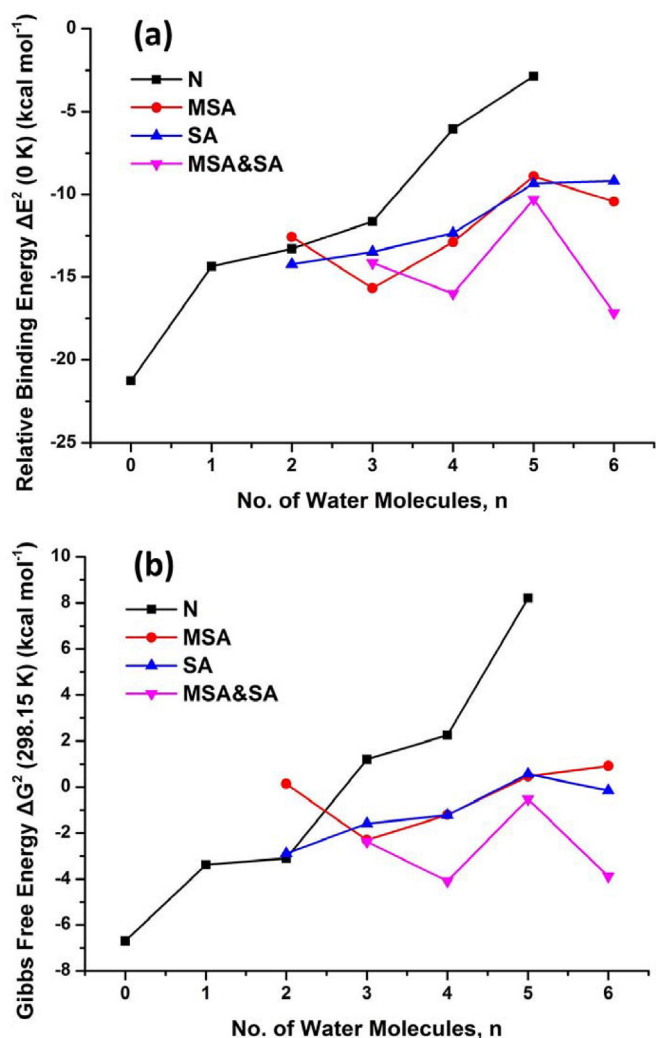


Fig. 3. Relative binding energy ΔE^2 (a) and Gibbs free energy ΔG^2 (b) in kcal mol⁻¹ at the PW91PW91/6-311++G (3df, 3pd) level of stepwise MSA-SA heterodimer hydrate growth of the neutral (N), di-ionic MSA⁻-SA-W⁺-W_{n-1} (MSA), di-ionic MSA-SA⁻-W⁺-W_{n-1} (SA), and tetra-ionic MSA⁻-SA⁻-(W⁺)₂-W_{n-2} (MSA&SA) via the route: MSA-SA-W_{n-1}+W→MSA-SA-W_n.

results also predict that the additional of MSA can promote the hydration of SA to form stable structures and that only few W molecules are needed to cause acid dissociation.

3.4. Temperature dependence and conformational population

The global minima have the greatest population in the ensemble of energetically accessible conformers at 0 K. However, as the systems grow, the energy differences between the global minima and other competing local minima decrease. In addition, the temperature also contributes to the stability of the isomers. Hence, studying the temperature dependence of the isomer contributions provides a more accurate picture of the relative isomer stabilities.

Previous studies (Mhin et al., 1993; Kim et al., 1994; Lee et al., 2000) have revealed that the thermodynamic properties of clusters depend on the temperatures and that the temperature contributes to cluster formation. For experimentalists, it is difficult to perform the relevant experiments at low temperatures due to the wall loss problem (Torpo et al., 2007). With quantum chemistry calculations, we can readily get such data, and the following results may aid in predicting the effect of temperature on the formation of MSA-SA-W_n (n = 1–6)

clusters.

The change in Gibbs free energy with temperatures from 50 to 400 K could have a large influence on the relative populations of different isomers; thus, an effect of temperature on the relative populations of isomers for MSA-SA-W_n (n = 1–6) is expected. The equations to calculate their relative populations at various temperatures are listed in follows:

$$P_n^i = \frac{\exp\left(-\frac{\Delta\Delta G_n^i}{RT}\right)}{\sum_i \exp\left(-\frac{\Delta\Delta G_n^i}{RT}\right)} \quad (2)$$

where

$$\Delta G_n^i = G_n^i - G^{MSA} - G^{SA} - nG^W \quad (3)$$

$$\Delta\Delta G_n^i = \Delta G_n^i - \min\{\Delta G_n^i\} \quad (4)$$

Here *n* and *i* represent the number of W molecules in a cluster and the isomer order, respectively. P_n^i is the relative population of the *i*th isomer at one cluster size, $\Delta\Delta G_n^i$ is the Gibbs free energy of the *i*th isomer compared to the most stable one, *R* is the ideal gas constant, and *T* is the temperature (Lv et al., 2014). The conformational population depending on the temperature variance for MSA-SA-W₁₋₆ is shown in Fig. 4. Since a number of isomers are obtained at each species size, several isomers were selected to study their temperature dependences. The criteria to choose the analyzed isomers were based on the isomers with: 1) different configuration types (surface type or interior type), 2) different acid-dissociation channels (N, MSA, SA, or MSA&SA), and 3) a different number of HBs formed in each clusters. Generally, the population of the lowest-energy isomer of each case of the MSA-SA-W_n clusters decreases, whereas the roles of other low-lying isomers become competitive as the temperature is increased.

For the case of the MSA-SA-W₁ cluster, as shown in Fig. 4 (a), the population of the minimum isomer (I-a) remains constant (almost 100%) at 50–200 K, then gradually decreases with increasing temperature up to 400 K. This isomer has a higher population than that of any other isomers at all temperatures. In addition to the global minimum structure (I-a), isomer I-i (N) increases in population starting from 300 K. The surface-type configurations I-b and I-c are more unfavorable than the interior-type configuration at all employed temperatures.

For MSA-SA-W₂, the population of isomers II-a and II-b crossover at approximately 250 K; the global minimum II-a has a higher population below 220 K, whereas isomer IV-b has a higher population above 250 K. In addition, isomer II-a also possesses an interior-type configuration with six HBs, whereas II-b possesses a surface-type configuration with five HBs. The conformational populations of the other isomers remain mainly unchanged with increasing temperature, showing a relatively weak temperature effect.

For the case of the MSA-SA-W₃ cluster, the global minimum isomer III-a is more prevalent than the other isomers below 100 K, but its predominance decreases thereafter. The populations of isomers III-b and III-e show similar temperature-dependence trend, showing increases below 100 K and then slightly decreases at 150 K–350 K (but still prevalent). The population of isomers III-b and III-c crossover at approximately 150 K, and isomer III-e has a slightly higher population than that of III-b. The population of isomer III-g gradually increases above 100 K, becomes competitive with those of III-b and III-e starting from 300 K, and finally becomes dominant at 400 K.

For MSA-SA-W₄, although the population of the minimum energy isomer IV-a (MSA&SA) gradually decreases with increasing temperature, it still remains higher than those of the other isomers at all temperatures, showing a similar trend as the MSA-SA-W₁ cluster and indicating that the two structures are relative stable and favorable. In addition, isomers IV-b and IV-c are competitive at high temperatures (200–400 K). The conformational populations of the other isomers are

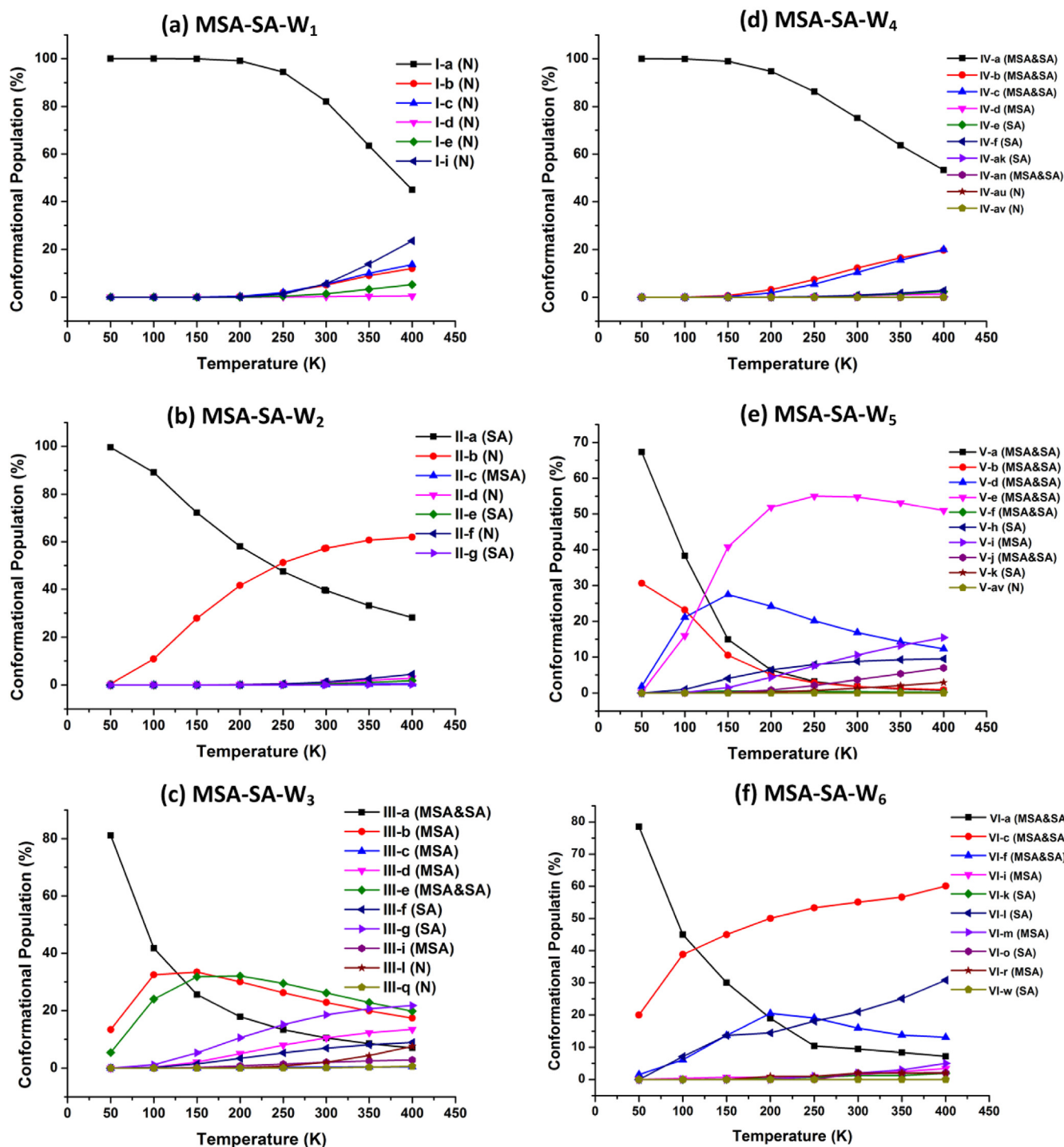


Fig. 4. The conformational population change for the low-lying isomers of the MSA-SA-W₁₋₆ clusters as a function of the temperature from 50 K to 400 K.

insensitive to increasing temperature.

Isomers V-a and V-b of the MSA-SA-W₅ cluster occupy the clear majority of conformational population, i.e., 70% and 30%, respectively, and then, the populations of these isomers gradually decrease to almost zero. Meanwhile, starting at 50 K, the population of isomer V-e sharply increases with increasing temperature and exceeds those of the other local minima at approximately 125 K, receiving its highest conformational population at 250 K (55%) before remaining constant upon further temperature increase. The population of isomer V-d also shows a temperature effect, as the population increases from 0% to 25% and

then decreases to 13% at 400 K.

For MSA-SA-W₆, the populations of isomers VI-a and VI-b crossover at approximately 110 K; the global minimum VI-a has the highest population below 110 K, while isomer VI-b has the highest population above 110 K and keeps its predominance at the rest of other temperatures. The population of isomers VI-f and VI-l are competitive at relatively low temperatures (50–250 K), and then the population of isomer VI-l increases, whereas the population of isomer VI-f decreases at 300–400 K. The populations of the other isomers remain unchanged with the temperature variance.

In general, the global minima of the smaller sized clusters are prevalent throughout the entire temperature range. As the temperature increases, the populations of the global minima decrease, whereas those of the other local minima increase. The ionic clusters with MSA dissociation and/or SA dissociation are more prevalent than their neutral counterparts, especially at lower temperatures, e.g., below 250 K for the MSA–SA–W₂ cluster. Moreover, the structures with interior-type configurations are also dominant over those with surface-type configurations. Similarly, clusters with more intermolecular HBs are more prevalent in the cluster population. That is, the structures with ionic, interior-type configurations and more HBs prevail within the experimental temperature range, and the other types of configurations may also be present in some proportions. Temperature effects could contribute to an alternation of the stability order of the isomers. However, the stability patterns for the MSA–SA–W_{1–6} system are significantly different with different number of W molecules due to their considerably different Gibbs free energy values among the stable minima, which also reflect the different shapes of their potential energy surfaces (Jiang et al., 2014). In addition, for the MSA–SA–W₁ and MSA–SA–W₄ clusters, the global minima are the most prevalent among all isomers at all temperatures, indicating the stable nature of these isomers.

3.5. Atmospheric relevance

The formation free energy of the heterodimer cluster MSA–SA at 298.15 K (−6.72 kcal mol^{−1}) suggests that MSA could contribute to the aerosol nucleation process by effectively binding to SA, the dominant nucleating species in the atmosphere. It is very interesting to determine the actual concentrations of the various hydrated MSA–SA clusters to investigate their effects in realistic atmospheric conditions, as the real concentrations can provide possible references for the existence of these clusters in the atmosphere.

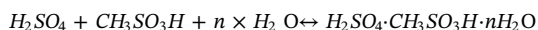
As shown in section 3.4, there are always some isomers have some percentage at various temperatures for each size clusters. Considering the Boltzmann distribution of the lower energy isomers, so we used the Boltzmann averaged Gibbs free energy to study the flatness of the potential energy surface of MSA–SA–W_n (n = 1–6) clusters. The Boltzmann averaged Gibbs free energy was derived from equation (2), which is listed in follows:

$$\Delta G_n^B = \sum_i p_n^i \Delta G_n^i \quad (5)$$

From the Boltzmann averaged Gibbs free energy ΔG_n^B (298.15 K), the equilibrium constant K_n for the formation of the cluster from the respective monomers is given:

$$K_n = \exp\left(\frac{-\Delta G_n^B}{RT}\right) \quad (6)$$

For the reaction,



the equilibrium constant K_n is also defined by

$$K_n = \frac{[SA\Delta MSA\Delta nW]}{[W]^n [MSA][SA]} \quad (7)$$

The value of the relative population fraction (RPF) is then defined by:

$$RPF = \frac{[SA\Delta MSA\Delta nW]}{[MSA][SA]} = K_n [W]^n \quad (8)$$

The typical concentration of SA in the atmosphere is in the range of 10⁵ to 10⁷ molecules cm^{−3} (Kulmala and Kerminen, 2008; Smith et al., 2008), and gas-phase MSA has been measured in air at concentrations that are approximately 10–100% of the co-existing gas-phase SA (Eisele and Tanner, 1993). In the current study, to access actual concentrations of the hydrated clusters, we assumed that the concentrations of SA and

Table 3

Boltzmann averaged Gibbs free energy (kcal mol^{−1}), Relative bound percentages (RPF × 100%) and estimated concentrations of each species of SA–MSA–W_n (n = 1–6). The estimated atmospheric concentrations (molecules cm^{−3}) are based on an SA concentration of 5 × 10⁶ molecules cm^{−3}, and an MSA concentration of 2.5 × 10⁶ molecules cm^{−3}.

Clusters	Boltzmann averaged Gibbs free energy (kcal mol ^{−1})	Relative Bound Percentages (RPF × 100%)	Concentrations (molecules cm ^{−3})
SA-MSA	−6.72	8.47 × 10 ^{−8}	1.06 × 10 ⁶
SA-MSA-W ₁	−9.73	1.37 × 10 ^{−11}	1.71 × 10 ²
SA-MSA-W ₂	−12.97	3.24 × 10 ^{−24}	4.05 × 10 ^{−11}
SA-MSA-W ₃	−14.94	9.07 × 10 ^{−35}	1.13 × 10 ^{−21}
SA-MSA-W ₄	−18.34	2.84 × 10 ^{−43}	3.55 × 10 ^{−30}
SA-MSA-W ₅	−18.81	6.31 × 10 ^{−50}	7.89 × 10 ^{−37}
SA-MSA-W ₆	−22.19	1.90 × 10 ^{−59}	2.38 × 10 ^{−46}

MSA were 5 × 10⁶ molecules cm^{−3} and 2.5 × 10⁶ molecules cm^{−3}, respectively. From the relative populations of the monomers and the equilibrium constants K_n using ΔG_n^B values at 298.15 K, the PRF values and the concentrations of the hydrated clusters in the atmosphere were estimated, as shown in Table 3. The approximations in this study are limited and simplistic, as it is hard to precisely describe the situations in the atmosphere since the real condition are much more complicated. However, we think the assumptions are useful to get a feel for how important these clusters are in the formation of aerosols.

As shown in Table 2, W molecules can easily bind to the MSA–SA dimer core based on the favorable stepwise formation free energies of the MSA–SA–W_n (n = 1–6) clusters, which suggests that these clusters promote the aerosol formation process. The MSA–SA dimer was calculated to have a concentration of 1.06 × 10⁶ molecules cm^{−3}. The large concentration of the dimer further demonstrates the significance of the MSA–SA cluster in the atmosphere. However, the concentrations of the clusters gradually decrease with the binding of more W molecules. With W molecules n > 1, their low populations make them have negligible contribution to the atmospheric population.

A previous study (Loukonen et al., 2010) showed that the number of binding W molecules in the clusters can be affected by variations in the RH. To study the population changes with variations in the RH, the hydrate distributions of the MSA–SA heterodimer were estimated at various RHs. As an n-hydrate in this study, its relative concentration is defined by:

$$\begin{aligned} \frac{\rho(1, n)}{\rho_{MSA-SA}^{total}} &= \frac{\rho(1, n)}{[\rho(1,0) + \rho(1,1) + \dots + \rho(1,6)]} \\ &= \frac{K_1 K_2 \dots \left(S \times \frac{p_W^{eq}}{P}\right)^n}{\left[K_0 + K_1 \left(S \times \frac{p_W^{eq}}{P}\right) + \dots + K_1 K_2 \dots K_6 \left(S \times \frac{p_W^{eq}}{P}\right)^6\right]} \end{aligned} \quad (9)$$

Here, K_n is the equilibrium constant for the formation of an n-hydrate from one W molecule and the (n-1)-hydrate, which is calculated based on the Boltzmann averaged Gibbs free energy; ρ represents the concentration of different species, and S is the saturation ratio, which is defined as the ratio of the proper partial pressure of water vapor to the saturation vapor pressure P_W^{eq} ; thus, RH is defined as $RH = 100\% \times S$, and the reference pressure (P) is 1 atm (Noppel et al., 2002; Loukonen et al., 2010; Temelso et al., 2012a; Bustos et al., 2014). The hydration level, n , can be any value between 1 and 6.

We calculated the composition of the hydrates as a function of the initial MSA–SA heterodimer at different RHs with a constant temperature of 298.15 K, as shown in Fig. 5. For the non-hydrated MSA–SA heterodimer, the population of the cluster gradually decreases at the RH increases from 20% to 50%–80% to 100%. The population decrease is not very much at 20% RH (99%), and then, the population decreases to

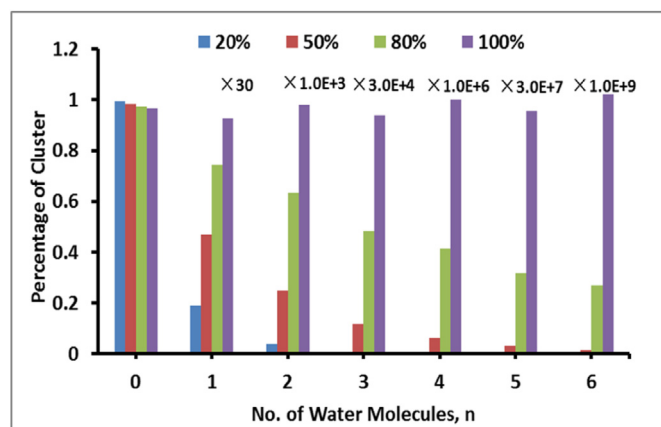


Fig. 5. Hydrated distributions of the clusters with MSA-SA heterodimers at four different relative humidities (RHs) of 20%, 50%, 80%, and 100%. The values on each column represent the corresponding amplification factor.

98% and 97% at 50% RH and 80% RH, respectively. The population of the hydrated clusters significantly decreases and possesses extremely low abundance at 20% RH. To directly compare the difference between the dimer and the hydrated clusters, all population intensities of the hydrated clusters under different RHs were amplified by a certain factor, as marked in Fig. 5. The most predominant hydrated cluster is the monohydrated cluster; however, its abundance is very low compared to that of the MSA-SA dimer (0.03% at an RH of 100%). The following general trend is observed in all cases: as the number of W molecules increases, the population of the hydrated clusters increases at a RH 20%–50% to 80%. Similarly, for $n > 2$ W molecules, their low populations make them negligible.

The sensitivity of the hydrate distributions to the RH was obvious. At the most tropospherically relevant conditions (RH and T), the total concentration of the MSA-SA dimer in these clusters was mainly distributed into non-hydrated species and monohydrates, and the monohydrate is more favorable than the other hydrates.

3.6. Parameters in kinetic code: evaporation rate

The Gibbs free energies can give us an idea of the relative stability of the clusters, but to compare them directly with experimental results, we need to include kinetics. This can be done through simple kinetic codes. Generally, a kinetic code is a bridge between the quantum chemical calculations and experiments. To include quantum chemical results in kinetic codes, first, the formation free energies need to be converted into cluster evaporation rates.

The following equation for the evaporation rate $\gamma_{i(i+j)}$, derived by Ortega et al. (Kupiainen et al., 2012; Ortega et al., 2012) was used in our analysis:

$$\gamma_{i(i+j)} = b_{ij} \frac{p}{k_B T n_0} \exp\left(\frac{\Delta G_{i+j} - \Delta G_i - \Delta G_j}{k_B T}\right) \quad (10)$$

where n_0 is the initial number of molecules in a cluster, $\gamma_{i(i+j)}$ is the evaporation rate of the i th-molecule from a cluster $i + j$, b_{ij} is the collision rate of the i th-molecule with the j th-molecule, ΔG_{i+j} , ΔG_i , and ΔG_j are the Gibbs free energies of formation of a molecule/cluster formed from monomers (molecules) at the reference pressure p . $\Delta G_{i+j} - \Delta G_i - \Delta G_j$ corresponds to the change in the Gibbs free energy of the system due to the attachment of the i th particle to the j th particle. Note that Eq. (10) describes the actual rate of removal of molecules from the surface of the droplet, which is equal to the rate of condensing molecules in the equilibrium state.

Assuming that the clusters are in a state of thermodynamic equilibrium, the collision rate b_{ij} between molecules/clusters can be estimated from (Kupiainen et al., 2012; Ortega et al., 2012):

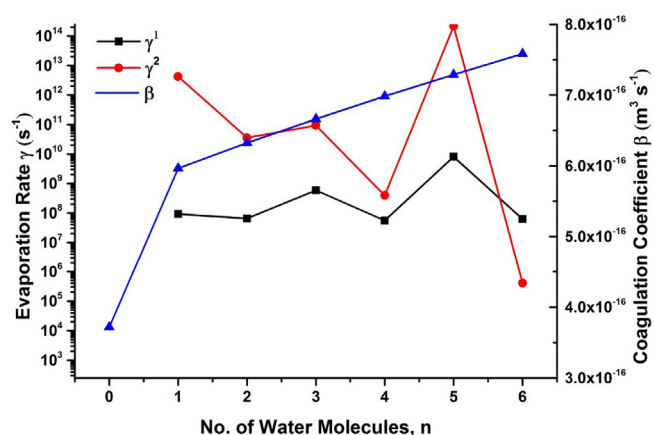


Fig. 6. The coagulation coefficient/collision rate β (unit: $\text{m}^{-3} \text{s}^{-1}$) and evaporation rates γ^1 and γ^2 (unit: s^{-1}) of a single water evaporation pathway of the MSA-SA- W_n clusters calculated under two different Gibbs free energy of formation equations: ΔG_B^1 (Boltzmann averaged Gibbs free energies), and ΔG^2 ($\Delta G^2 = G_n - G_{\text{MSA-SA-(n-1)W}} - G_W$).

$$b_{ij} = (8\pi k_B T)^{1/2} \left(\frac{1}{m_i} + \frac{1}{m_j} \right)^{1/2} (r_i + r_j)^2 \quad (11)$$

where m_i and m_j are the masses of the i th molecule and j th molecules/cluster and r_i and r_j are their radii. Here, we have assumed that only single molecules can stick to clusters and evaporate from them and that processes involving more than one cluster can be neglected.

The coagulation coefficient, also called the collision rate β , and the evaporation rates γ of a single water evaporation pathway of the MSA-SA- W_n clusters were calculated under two different free energy of formation equations, ΔG_B^1 (Boltzmann averaged Gibbs free energies) and ΔG^2 ($\Delta G^2 = G_n - G_{\text{MSA-SA-(n-1)W}} - G_W$, based on the minimum energy structures). The corresponding γ^1 and γ^2 are shown in Fig. 6. The collision rate β is gradually increases with an increasing cluster size within the same order of magnitude of $\sim 10^{-16}$. Quite large discrepancies between ΔG_B^1 and ΔG^2 are found: the ΔG_B^1 values monotonously increase with an increase in the number of W molecules, whereas the ΔG^2 values are fluctuant and irregular between the species. Moreover, the ΔG^2 value of MSA-SA- W_5 is found to be positive. The obvious difference between ΔG_B^1 and ΔG^2 results in the large difference in evaporation rates γ^1 and γ^2 . Although the trend in the changes of the evaporation rates under the two calculated Gibbs free energies are consistent with each other, the maximum difference between the two methods is more than several orders of magnitude, observed in the MSA-SA- W_1 cluster which has the lowest degree of hydration. Both calculation methods indicate that the MSA-SA- W_5 cluster is unstable and its W molecules is readily evaporated compared to the other clusters. The most stable and hence longest-lived clusters overall are MSA-SA- W_4 and MSA-SA- W_6 with their highest evaporation rates (from a single water evaporation pathway) of $5.52 \times 10^7 \text{ s}^{-1}$ and $6.20 \times 10^7 \text{ s}^{-1}$, respectively. The values are considerably smaller than the neighboring MSA-SA- W_5 cluster.

Previous study (Chen et al., 2017) of oxalic acid-dimethylamine-water (OA-DMA- W_n , $n = 1-4$) system have shown that the evaporation of water is more significant than the evaporation of OA or DMA molecules. The evaporation rate from OA-DMA- W_1 to OA-DMA- W_4 was ranged between 10^8 and 10^{12} s^{-1} , presenting a periodic fluctuation trend, which is consistent with our results. Recently, Miao et al. (2018) thoroughly studied the systems of the (MSA $^-$) (NH_3 /amines: MA, DMA, TMA) (H_2O) $_n$ ($n = 1-3$), and they found that the change in evaporation rate for water is different for the different systems, in the (MSA $^-$) (amines: MA, DMA, TMA) (H_2O) $_n$ ($n = 1-3$) clusters, they increase monotonically with the added water (from 10^6 and 10^9 s^{-1}), which is different from our non-monotonic changes in the MSA-SA- W_n system.

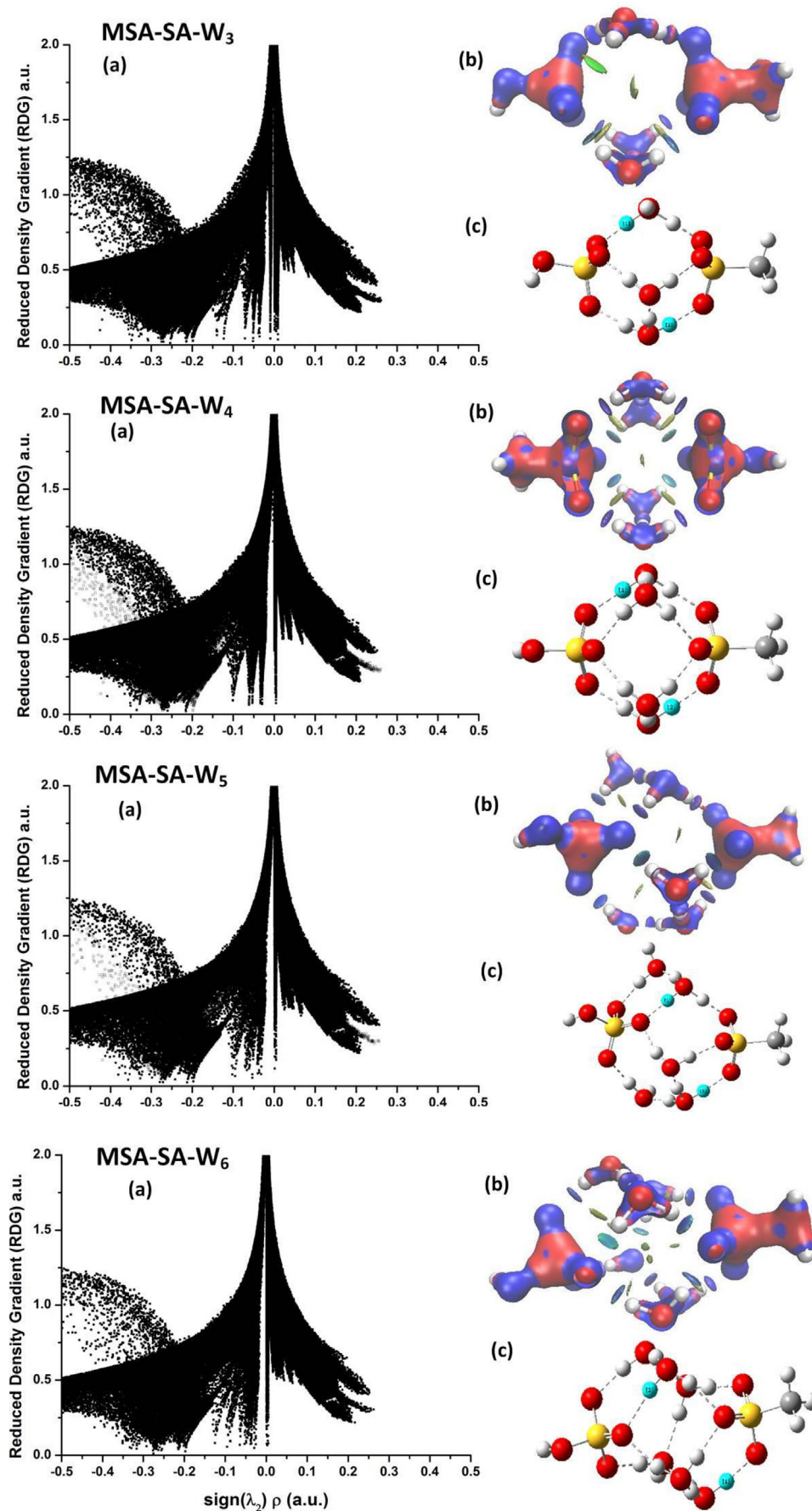


Fig. 7. Noncovalent interactions: the electron density ($\text{sign}(\lambda_2) \rho$) as a function of the reduced density gradient (RDG) (a) and the visualized weak intermolecular interactions (b) of the minimum energy isomer of the MSA-SA- W_n , $n = 3-6$ cluster (c).

In the current study, it can be clearly seen that the evaporation rates depend exponentially on the free energy of formation, which means that the accuracy of these calculations is very important and is deserved to be the subject of further study. Very recently, the high sensitivity of the evaporation rates on the shape and the mode of the experimentally observed particle size distributions are demonstrated for the related system of H_2SO_4 clusters by Zeuch et al. (Carlsson and Zeuch, 2018). In addition, this analysis method can be extended to allow a direct validation of quantum chemically predicted stabilities of small H_2SO_4 clusters. This also provides us with a possible direction for obtaining accurate kinetic data and evaporation rates in the further study.

3.7. Intermolecular interactions

Topological analysis of the electron density can prove the existence of the hydrogen bond in all clusters. From the above analysis, we found that the structures of the MSA-SA-W_n clusters are favorable and relative stable; therefore, it is necessary to determine their intermolecular and intramolecular interactions.

The non-covalent interaction (NCI) index is based on the relationship between the electron density and the reduced density gradient (RDG) and was proposed by Yang and coworkers (Johnson et al., 2010; Contreras-García et al., 2011). By means of the RDG, the non-covalent interactions and covalent interactions in real space can be confirmed. The plot of the RDG versus the electron density multiplied by the sign of the second Hessian eigenvalue (sign $(\lambda_2) \rho$) and the reduced gradient isosurfaces ($s = 0.05$ a. u.) generated for MSA-SA-W_n , $n = 3-6$ are shown in Fig. 7 (a) and (b) based on the structure shown in Fig. 7 (c). The calculations were employed using the Multiwfn program (T. T. Lu, 2010) and visualized by the VMD program (Humphrey et al., 1996).

In Fig. 7 (a), it is clear that the difference between the different systems (MSA-SA-W_n , $n = 3-6$ clusters) is not much, the sign $(\lambda_2) \rho$ values for the left spike are negative, corresponding to strong hydrogen bonds. In addition, these spikes look very compact, which indicate that the lattices are reasonably set up. The sign $(\lambda_2) \rho$ values for the right spike are positive, corresponding to the steric effect region in the cage (also called non-bonded overlap). For all the MSA-SA-W_n , $n = 3-6$ clusters, the presented steric effects (right spikes) are not as strong as the left spike, indicating that the weak interactions are dominant.

The corresponding isosurfaces are shown in Fig. 7 (b), where the green to blue color-coded regions of the bonding isosurface indicate where the hydrogen-bonding interaction is becoming stronger. From MSA-SA-W_3 to MSA-SA-W_6 cluster, the color coding of these bonding isosurfaces demonstrates that the stability order of the hydrogen bonding interactions for different clusters is $\text{MSA-SA-S-W}_4 > \text{MSA-SA-W}_6 > \text{MSA-SA-W}_5 > \text{MSA-SA-W}_3$, which is similar to the results of evaporation rates. In the regions between the intermolecular oxygen and hydrogen atoms and the intramolecular oxygen and hydrogen atoms, blue isosurfaces exist, corresponding to strong hydrogen bonds, which are in the left spike in Fig. 7 (a). Here, it is observed that both stronger and weaker intermolecular hydrogen bonds exist in all the MSA-SA-W_n ($n = 3-6$) systems. Some intermolecular hydrogen bonds are relatively stronger; the phenomenon of proton transfer can also be seen.

4. Conclusions

In the current study, the interaction of MSA with SA in presence of W has been investigated using DFT calculations to study the mechanism of ternary nucleation from a microscopic aspect. The structure of the monomers and heterodimers agreed well with earlier reports, an ionization events and cluster growth were also studied. The present study led to following findings:

- (a) MSA-SA-W_{0-6} clusters exhibit obvious structural evolution from the heterodimer to the largest hydrated cluster MSA-SA-W_6 . The W

molecules prefer to bridge in the middle of MSA and SA to form an interior-type configuration. In addition, the system also exhibit very strong hydrogen bonds. The first deprotonation of MSA or SA begins once the second W molecule is added to the MSA-SA-W_1 complex; upon the addition of more W molecules, dissociation occurs in MSA and SA simultaneously. The tetra-ionic clusters are more stable than the di-ionic clusters and neutral clusters.

- (b) The thermodynamics and concentration results indicate that MSA probably forms clusters with SA in the atmosphere. From an analysis of the contributions of various isomers to the conformational populations, the lowest energy states are observed to have higher concentrations than the other isomers of the same size for the MSA-SA-W_1 and MSA-SA-W_4 clusters at all employed temperatures. Thus, the small populations of the configurations with lower energies can be ignored. For other cluster sizes, the low-lying isomers compete with the minima upon variations in the temperature. An obvious concentration of the MSA-SA cluster is predicted to be present in the atmosphere, and these clusters could likely participate in the process of new particle formation. However, the concentration of clusters gradually decreases upon the binding of more W molecules. The larger sized clusters show infinitesimal populations at typical boundary-layer atmospheric temperature, which could result in relatively lower concentration in the atmosphere.
- (c) Our study serves as the first kinetic investigation of MSA-SA-W_{1-6} clusters. The evaporation rates are calculated for a single W molecule evaporation pathway. We found that the evaporation rates depend exponentially on the free energy of formation; however, the changes of evaporation rate under two different Gibbs free energies are consistent with each other. The maximum difference is found in the MSA-SA-W_1 cluster (approximately five orders of magnitude); thus, the accuracy of the free energy of formation calculations is very important. In addition, we found that the structures of the MSA-SA-W_n clusters are favorable and relative stable; the non-covalent interactions of MSA-SA-W_{3-6} cluster were thoroughly studied.

The current work is fundamental and necessary for our further study of pre-nucleation clusters containing a mixture of MSA, SA and W. This work predicts the possible forms of MSA with SA in presence of W during nucleation from a theoretical approach. More theoretical and experimental studies are still needed to elucidate the nucleation mechanism.

Acknowledgements

This work was supported by the National Natural Science Foundation of China (Grant No. 41775122, 21403244, 21573241, 41605099, 41705097, 41705111, 41775112 and 41527808), the National Science Fund for Distinguished Young Scholars (Grant No. 41725019), Key Research Program of Frontier Science, CAS (Grant No. QYZDB-SSW-DQC031), the Key Research Program of the Chinese Academy of Sciences (Grant No. ZDRW-ZS-2016-4-3-6) and the National Key Research and Development program (Grant No. 2016YFC0202203 and 2016YFC0202703), and the National Research Program for Key Issues in Air Pollution Control (DQGG0103).

Appendix A. Supplementary data

Supplementary data related to this article can be found at <https://doi.org/10.1016/j.atmosenv.2018.07.050>.

References

- Aalto, P., Hameri, K., Becker, E., Weber, R., Salm, J., Makela, J.M., Hoell, C., O'Dowd, C.D., Karlsson, H., Hansson, H.C., Vakeva, M., Koponen, I.K., Buzorius, G., Kulmala, M., 2001. Physical characterization of aerosol particles during nucleation events.

- Tellus B 53 (4), 344–358.
- Bork, N., Elm, J., Olenius, T., Vehkamäki, H., 2014. Methane sulfonic acid-enhanced formation of molecular clusters of sulfuric acid and dimethyl amine. *Atmos. Chem. Phys.* 14 (22), 12023–12030.
- Bustos, D.J., Temelso, B., Shields, G.C., 2014. Hydration of the sulfuric acid-methylamine complex and implications for aerosol formation. *J. Phys. Chem.* 118 (35), 7430–7441.
- Carlsson, P.T.M., Zeuch, T., 2018. Investigation of nucleation kinetics in H₂SO₄ vapor through modeling of gas phase kinetics coupled with particle dynamics. *J. Chem. Phys.* 148, 104303.
- Charlson, R.J., Schwartz, S.E., Hales, J.M., Cess, R.D., Coakley, J.A., Hansen, J.E., Hofmann, D.J., 1992. Climate forcing by anthropogenic aerosols. *Science* 255 (5043), 423–430.
- Chen, H., Ezell, M.J., Arquero, K.D., Varner, M.E., Dawson, M.L., Gerber, R.B., Finlayson-Pitts, B.J., 2015. New particle formation and growth from methanesulfonic acid, trimethylamine and water. *Phys. Chem. Chem. Phys.* 17 (20), 13699–13709.
- Chen, J., Jiang, S., Liu, Y.R., Huang, T., Wang, C.Y., Miao, S.K., Wang, Z.Q., Zhang, Y., Huang, W., 2017. Interaction of oxalic acid with dimethylamine and its atmospheric implications. *RSC Adv.* 7 (11), 6374–6388.
- Contreras-Garcia, J., Yang, W., Johnson, E.R., 2011. Analysis of hydrogen-bond interaction potentials from the electron density: integration of noncovalent interaction regions. *J. Phys. Chem.* 115 (45), 12983–12990.
- Dawson, M.L., Varner, M.E., Perraud, V., Ezell, M.J., Gerber, R.B., Finlayson-Pitts, B.J., 2012. Simplified mechanism for new particle formation from methanesulfonic acid, amines, and water via experiments and ab initio calculations. *P. Natl. Acad. Sci. USA* 109 (46), 18719–18724.
- Delley, B., 1990. An all-electron numerical-method for solving the local density functional for polyatomic-molecules. *J. Chem. Phys.* 92 (1), 508–517.
- Eisele, F.L., Tanner, D.J., 1993. Measurement of the gas-phase concentration of H₂SO₄ and methanesulfonic-acid and estimates of H₂SO₄ production and loss in the atmosphere. *J. Geophys. Res. Atmos.* 98 (D5), 9001–9010.
- Ezell, M.J., Johnson, S.N., Yu, Y., Perraud, V., Bruns, E.A., Alexander, M.L., Zelenyuk, A., Dabdub, D., Finlayson-Pitts, B.J., 2010. A new aerosol flow system for photochemical and thermal studies of tropospheric aerosols. *Aerosol Sci. Technol.* 44 (5), 329–338.
- Fan, J., Zhang, R., Collins, D., Li, G., 2006. Contribution of secondary condensable organics to new particle formation: a case study in Houston, Texas. *Geophys. Res. Lett.* 33 (15), L15802.
- Forbert, H., Masia, M., Kaczmarek-Kedziera, A., Nair, N.N., Marx, D., 2011. Aggregation-Induced chemical reactions: acid dissociation in growing water clusters. *J. Am. Chem. Soc.* 133 (11), 4062–4072.
- Frisch, M.J., Schlegel, H.B., Scuseria, G.E., Robb, M.A., Scalmani, G., Barone, V., Mennucci, B., Petersson, G.A., Caricato, M., Li, X., Hratchian, H.P., Izmaylov, A.F., Zheng, G., Sonnenberg, J.L., Hada, M., 2009. Gaussian 09, Revision A.02. Gaussian, Inc., Wallingford CT.
- Gutberlet, A., Schwaab, G., Birer, O., Masia, M., Kaczmarek, A., Forbert, H., Havenith, M., Marx, D., 2009. Aggregation-induced dissociation of HCl(H₂O)₄ below 1 K: the smallest droplet of acid. *Science* 324 (5934), 1545–1548.
- Humphrey, W., Dalke, A., Schulten, K., 1996. VMD: visual molecular dynamics. *J. Mol. Graph. Model.* 14 (1), 33–38.
- Jiang, S., Huang, T., Liu, Y.R., Xu, K.M., Zhang, Y., Lv, Y.Z., Huang, W., 2014. Theoretical study of temperature dependence and Rayleigh scattering properties of chloride hydration clusters. *Phys. Chem. Chem. Phys.* 16 (36), 19241–19249.
- Johnson, E.R., Keinan, S., Mori-Sanchez, P., Contreras-Garcia, J., Cohen, A.J., Yang, W., 2010. Revealing noncovalent interactions. *J. Am. Chem. Soc.* 132 (18), 6498–6506.
- Kim, J.S., Mhin, B.J., Lee, S.J., Kim, K.S., 1994. Entropy-driven structures of the water octamer. *Chem. Phys. Lett.* 219 (3–4), 243–246.
- Kreidenweis, S.M., Flagan, R.C., Seinfeld, J.H., Okuyama, K., 1989. Binary nucleation of methanesulfonic-acid and water. *J. Aerosol Sci.* 20 (5), 585–607.
- Kreidenweis, S.M., Seinfeld, J.H., 1988. Nucleation of sulfuric-acid water and methanesulfonic-acid water solution particles-implications for the atmospheric chemistry of organosulfur species. *Atmos. Environ.* 22 (2), 283–296.
- Kuang, C., Riipinen, I., Sihto, S.L., Kulmala, M., McCormick, A.V., McMurry, P.H., 2010. An improved criterion for new particle formation in diverse atmospheric environments. *Atmos. Chem. Phys.* 10 (17), 8469–8480.
- Kulmala, M., 2003. How particles nucleate and grow. *Science* 302 (5647), 1000–1001.
- Kulmala, M., Kerminen, V.M., 2008. On the formation and growth of atmospheric nanoparticles. *Atmos. Res.* 90 (2–4), 132–150.
- Kupiainen, O., Ortega, I.K., Kurten, T., Vehkamäki, H., 2012. Amine substitution into sulfuric acid - ammonia clusters. *Atmos. Chem. Phys.* 12 (8), 3591–3599.
- Lee, H.M., Suh, S.B., Lee, J.Y., Tarakeshwar, P., Kim, K.S., 2000. Structures, energies, vibrational spectra, and electronic properties of water monomer to decamer. *J. Chem. Phys.* 112 (22), 9759–9772.
- Leopold, K.R., 2011. Hydrated acid clusters. *Annu. Rev. Phys. Chem.* 62, 327–349.
- Li, S., Qian, W., Tao, F.-M., 2007a. Ionic dissociation of methanesulfonic acid in small water clusters. *Chem. Phys. Lett.* 438 (4–6), 190–195.
- Li, S., Zhang, L., Qin, W., Tao, F.-M., 2007b. Intermolecular structure and properties of the methanesulfonic acid-ammonia system in small water clusters. *Chem. Phys. Lett.* 447 (1–3), 33–38.
- Liu, Y.R., Wen, H., Huang, T., Lin, X.X., Gai, Y.B., Hu, C.J., Zhang, W.J., Huang, W., 2014. Structural exploration of water, nitrate/water, and oxalate/water clusters with basin-hopping method using a compressed sampling technique. *J. Phys. Chem.* 118 (2), 508–516.
- Loukonen, V., Kurten, T., Ortega, I.K., Vehkamäki, H., Padua, A.A.H., Sellegri, K., Kulmala, M., 2010. Enhancing effect of dimethylamine in sulfuric acid nucleation in the presence of water - a computational study. *Atmos. Chem. Phys.* 10 (10), 4961–4974.
- Lu, T., 2010. Multiwfn: a Multifunctional Wavefunction Analyzer, Version 3.0.1. 2010. <http://multiwfn.codeplex.com>.
- Lv, Z.L., Xu, K., Cheng, Y., Chen, X.R., Cai, L.C., 2014. Ab initio investigation of the lower energy candidate structures for (H₂O)₅⁺ water cluster. *J. Chem. Phys.* 141 (5), 054309.
- McGraw, R., Zhang, R., 2008. Multivariate analysis of homogeneous nucleation rate measurements. Nucleation in the p-toluic acid/sulfuric acid/water system. *J. Chem. Phys.* 128 (6), 064508.
- Mhin, B.J., Lee, S.J., Kim, K.S., 1993. Water cluster distribution with respect to pressure and temperature in the gas-phase. *Phys. Rev.* 48 (5), 3764–3770.
- Miao, S.K., Jiang, S., Chen, J., Ma, Y., Zhu, Y.P., Wen, Y., Zhang, M.M., Huang, W., 2015. Hydration of a sulfuric acid-oxalic acid complex: acid dissociation and its atmospheric implication. *RSC Adv.* 5 (6), 48638–48646.
- Miao, S.K., Jiang, S., Peng, X.Q., Liu, Y.R., Feng, Y.J., Wang, Y.B., Zhao, F., Huang, T., Huang, W., 2018. Hydration of the methanesulfonate-ammonia/amine complex and its atmospheric implications. *RSC Adv.* 8 (6), 3250–3263.
- Molina, M.J., Molina, L.T., Zhang, R.Y., Meads, R.F., Spencer, D.D., 1997. The reaction of ClONO₂ with HCl on aluminum oxide. *Geophys. Res. Lett.* 24 (13), 1619–1622.
- Nadykto, A.B., Yu, F., 2007. Strong hydrogen bonding between atmospheric nucleation precursors and common organics. *Chem. Phys. Lett.* 435 (1–3), 14–18.
- Noppel, M., Vehkamäki, H., Kulmala, M., 2002. An improved model for hydrate formation in sulfuric acid-water nucleation. *J. Chem. Phys.* 116 (11), 218–228.
- O'Dowd, C., McFiggans, G., Creasey, D.J., Pirjola, L., Hoell, C., Smith, M.H., Allan, B.J., Plane, J.M.C., Heard, D.E., Lee, J.D., Pilling, M.J., Kulmala, M., 1999. On the photochemical production of new particles in the coastal boundary layer. *Geophys. Res. Lett.* 26 (12), 1707–1710.
- Ortega, I.K., Kupiainen, O., Kurten, T., Olenius, T., Wilkman, O., McGrath, M.J., Loukonen, V., Vehkamäki, H., 2012. From quantum chemical formation free energies to evaporation rates. *Atmos. Chem. Phys.* 12 (1), 225–235.
- Paasonen, P., Nieminen, T., Asmi, E., Manninen, H.E., Petaja, T., Plass-Duelmer, C., Flenje, H., Birmili, W., Wiedensohler, A., Horrak, U., Metzger, A., Hamed, A., Laaksonen, A., Facchini, M.C., Kerminen, V.M., Kulmala, M., 2010. On the roles of sulphuric acid and low-volatility organic vapours in the initial steps of atmospheric new particle formation. *Atmos. Chem. Phys.* 10 (22), 11223–11242.
- Perdew, J.P., Burke, K., Wang, Y., 1996. Generalized gradient approximation for the exchange-correlation hole of a many-electron system. *Phys. Rev. B* 54 (23), 16533–16539.
- Raghavachari, K., Trucks, G.W., 1989. Highly correlated systems – excitation-energies of 1st row transition-metals Sc-Cu. *J. Chem. Phys.* 91 (2), 1062–1065.
- Robertson, W.H., Johnson, M.A., 2002. Caught in the act of dissolution. *Science* 298 (5591), 69–69.
- Smith, J.N., Dunn, M.J., VanReken, T.M., Iida, K., Stolzenburg, M.R., McMurry, P.H., Huey, L.G., 2008. Chemical composition of atmospheric nanoparticles formed from nucleation in Tecamac, Mexico: evidence for an important role for organic species in nanoparticle growth. *Geophys. Res. Lett.* 35 (4), L04808.
- Temelso, B., Morrell, T.E., Shields, R.M., Allodi, M.A., Wood, E.K., Kirschner, K.N., Castonguay, T.C., Archer, K.A., Shields, G.C., 2012a. Quantum mechanical study of sulfuric acid hydration: atmospheric implications. *J. Phys. Chem.* 116 (9), 2209–2224.
- Temelso, B., Thuong Ngoc, P., Shields, G.C., 2012b. Computational study of the hydration of sulfuric acid dimers: implications for acid dissociation and aerosol formation. *J. Phys. Chem.* 116 (39), 9745–9758.
- Torpo, L., Kurten, T., Vehkamäki, H., Laasonen, K., Sundberg, M.R., Kulmala, M., 2007. Significance of ammonia in growth of atmospheric nanoclusters. *J. Phys. Chem.* 111 (42), 10671–10674.
- Vandingen, R., Raes, F., 1993. Ternary nucleation of methane sulfonic-acid, sulfuric-acid and water-vapor. *J. Aerosol Sci.* 24 (1), 1–17.
- Wang, L., Khalizov, A.F., Zheng, J., Xu, W., Ma, Y., Lal, V., Zhang, R., 2010. Atmospheric nanoparticles formed from heterogeneous reactions of organics. *Nat. Geosci.* 3 (4), 238–242.
- Weber, K.H., Morales, F.J., Tao, F.-M., 2012. Theoretical study on the structure and stabilities of molecular clusters of oxalic acid with water. *J. Phys. Chem.* 116 (47), 11601–11617.
- Wen, H., Hou, G.L., Kathmann, S.M., Valiev, M., Wang, X.B., 2013. Communication: solute anisotropy effects in hydrated anion and neutral clusters. *J. Chem. Phys.* 138 (3), 031101.
- Wen, H., Liu, Y.R., Xu, K.M., Huang, T., Hu, C.J., Zhang, W.J., Huang, W., 2014. Probing the 2D-to-3D structural transition in gold clusters with a single sulfur atom: AuxS^{0,+/-} (x = 1–10). *RSC Adv.* 4 (29), 15066–15076 2014.
- Wen, H., Hou, G.L., Liu, Y.R., Wang, X.B., Huang, W., 2016. Examining the structural evolution of bicarbonate-water clusters: insights from photoelectron spectroscopy, basin-hopping structural search, and comparison with available IR spectral studies. *Phys. Chem. Chem. Phys.* 18 (26), 17470–17482.
- Werner, J., Manby, G.K., Schuetz, M., 2010. Molpro, a Package of Ab Initio Program, Version 2010.1.
- Wyslouzil, B.E., Seinfeld, J.H., Flagan, R.C., Okuyama, K., 1991a. Binary nucleation in acid water-system. 1. Methanesulfonic-acid water. *J. Chem. Phys.* 94 (10), 6827–6841.
- Wyslouzil, B.E., Seinfeld, J.H., Flagan, R.C., Okuyama, K., 1991b. Binary nucleation in acid water-system. 2. Sulfuric-acid water and a comparison with methanesulfonic-acid water. *J. Chem. Phys.* 94 (10), 6842–6850.
- Xu, W., Zhang, R., 2012. Theoretical investigation of interaction of dicarboxylic acids with common aerosol nucleation precursors. *J. Phys. Chem.* 116 (18), 4539–4550.
- Xu, W., Zhang, R., 2013. A theoretical study of hydrated molecular clusters of amines and dicarboxylic acids. *J. Chem. Phys.* 139 (6), 064302.
- Zhang, R., 2010. Getting to the critical nucleus of aerosol formation. *Science* 328 (5984),

- 1366–1367.
- Zhang, R., Khalizov, A., Wang, L., Hu, M., Xu, W., 2012. Nucleation and growth of nanoparticles in the atmosphere. *Chem. Rev.* 112 (3), 1957–2011.
- Zhang, R., Li, G., Fan, J., Wu, D.L., Molina, M.J., 2007. Intensification of Pacific storm track linked to Asian pollution. *P. Natl. Acad. Sci. USA* 104 (13), 5295–5299.
- Zhang, R., Wang, L., Khalizov, A.F., Zhao, J., Zheng, J., McGraw, R.L., Molina, L.T., 2009. Formation of nanoparticles of blue haze enhanced by anthropogenic pollution. *P. Natl. Acad. Sci. USA* 106 (42), 17650–17654.
- Zhang, R.Y., Suh, I., Zhao, J., Zhang, D., Fortner, E.C., Tie, X.X., Molina, L.T., Molina, M.J., 2004. Atmospheric new particle formation enhanced by organic acids. *Science* 304 (5676), 1487–1490.
- Zhao, J., Levitt, N.P., Zhang, R.Y., 2005. Heterogeneous chemistry of octanal and 2,4-hexadienal with sulfuric acid. *Geophys. Res. Lett.* 32 (9), L09802.
- Zhao, J., Levitt, N.P., Zhang, R., Chen, J., 2006. Heterogeneous reactions of methylglyoxal in acidic media: implications for secondary organic aerosol formation. *Environ. Sci. Technol.* 40 (24), 7682–7687.
- Zhao, J., Khalizov, A., Zhang, R., McGraw, R., 2009. Hydrogen-bonding interaction in molecular complexes and clusters of aerosol nucleation precursors. *J. Phys. Chem.* 113 (4), 680–689.
- Zheng, J., Khalizov, A., Wang, L., Zhang, R., 2010. Atmospheric pressure-ion drift chemical ionization mass spectrometry for detection of trace gas species. *Anal. Chem.* 82 (17), 7302–7308.
- Zhu, Y.P., Liu, Y.R., Huang, T., Jiang, S., Xu, K.M., Wen, H., Zhang, W.J., Huang, W., 2014. Theoretical study of the hydration of atmospheric nucleation precursors with acetic acid. *J. Phys. Chem.* 118 (36), 7959–7974.